

Supplementary Information

Two Dimensional $\text{Ti}_3\text{C}_2\text{T}_x$ MXene Nanosheets for CO_2 Electroreduction in Aqueous DElectrolytes

Sarathkumar Krishnan^a, Senthilkumaran Marimuthu^a, Mayank K. Singh and Dhirendra K.

*Rai**

*Sustainable Energy & Environmental Materials (SEEM) Lab, Department of Metallurgical
Engineering and Materials Science (MEMS), Indian Institute of Technology Indore, Simrol,
Indore 453552, India.*

^a*Contributed equally to the work*

*Corresponding author: Tel: +91 731 660 3278

E-mail: dkrai@iiti.ac.in (D K Rai)

Table of contents

Figure S1. Schematic diagram of H-type cell

Figure S2. Powder-XRD patterns of Ti_3AlC_2 MAX phase and $\text{Ti}_3\text{C}_2\text{T}_x$

Figure S3. EDX spectra of $\text{Ti}_3\text{C}_2\text{T}_x$

Figure S4. ATR-FTIR spectrum of $\text{Ti}_3\text{C}_2\text{T}_x$ before and after CO_2 adsorption

Figure S5. LSV curves comparison $\text{Ti}_3\text{C}_2\text{T}_x$ -GCE at two different electrolyte concentrations such as 0.1 M KHCO_3 and 0.5 M KHCO_3

Figure S6. The pH values of the various concentration of KHCO_3 electrolytes before and after CO_2 purging

Figure S7. ^1H NMR spectra of products formed in electrolyte before and after 3 h

Figure S8. ^1H NMR spectra of products obtained from CA analysis with different potential (vs. Ag/AgCl) for 3 h.

Figure S9. Linearly fitted standard calibration curves for (a) acetone, (b) methanol and (c) ethanol

Figure S10. Gas chromatography profiles showing the formation of (a) CO, (b) H_2 and (c) overall CO_2 -reduced products carried out at the constant potential of -1.1 V (vs. Ag/AgCl) for 3 h.

Figure S11. Electrochemical double layer plot (scan rate vs. ΔJ) of modified $\text{Ti}_3\text{C}_2\text{T}_x$ -GCE

Table S1. Electrocatalytic properties $\text{Ti}_3\text{C}_2\text{T}_x$ -GCE with recently reported 2D materials towards C_1 and C_{2+} products.

Figure S12. (a) FE-SEM and (b) EDX spectrum of $\text{Ti}_3\text{C}_2\text{T}_x$ -GCE after 72 hr stability studies

Figure S13. Elemental mapping of $\text{Ti}_3\text{C}_2\text{T}_x$ -GCE after 72 hr stability studies

Figure S14. P-XRD pattern of $\text{Ti}_3\text{C}_2\text{T}_x$ -GCE before and after 72 hr electrolysis

Figure S15. Electrochemical impedance spectroscopy (EIS) of $\text{Ti}_3\text{C}_2\text{T}_x$ -GCE before and after 72 hr electrolysis

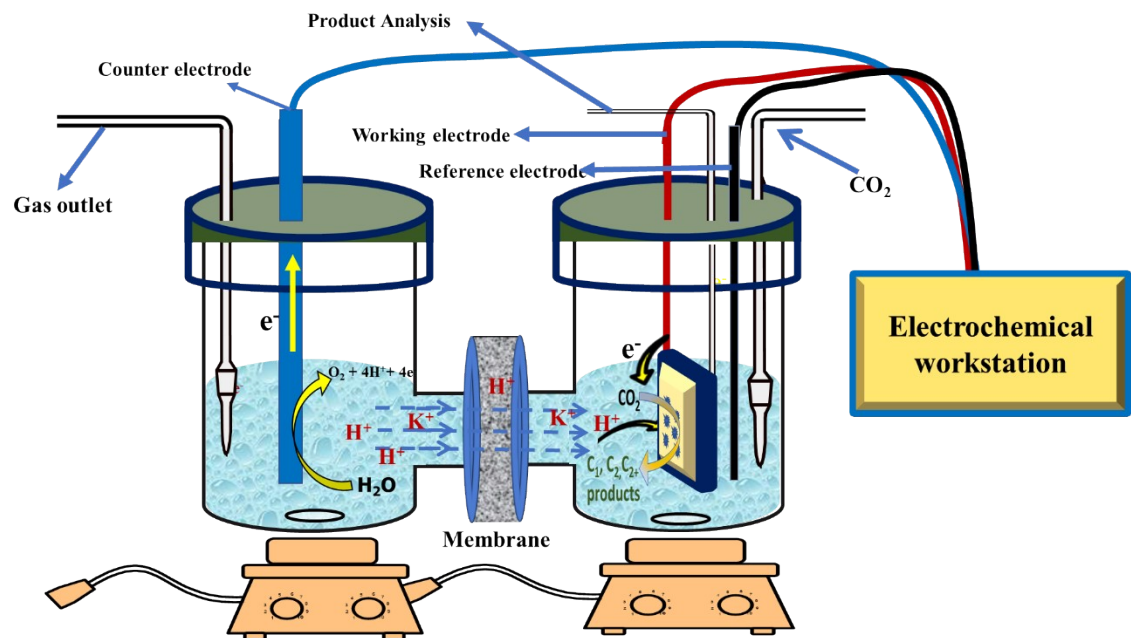


Figure S1. Schematic diagram of H-type cell

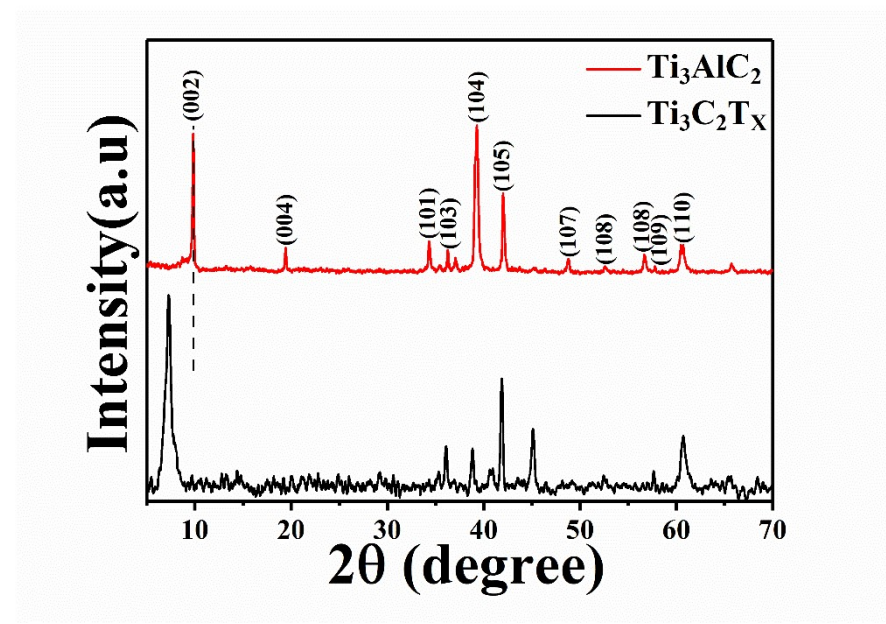


Figure S2. Powder-XRD patterns of Ti₃AlC₂ MAX phase and Ti₃C₂T_x

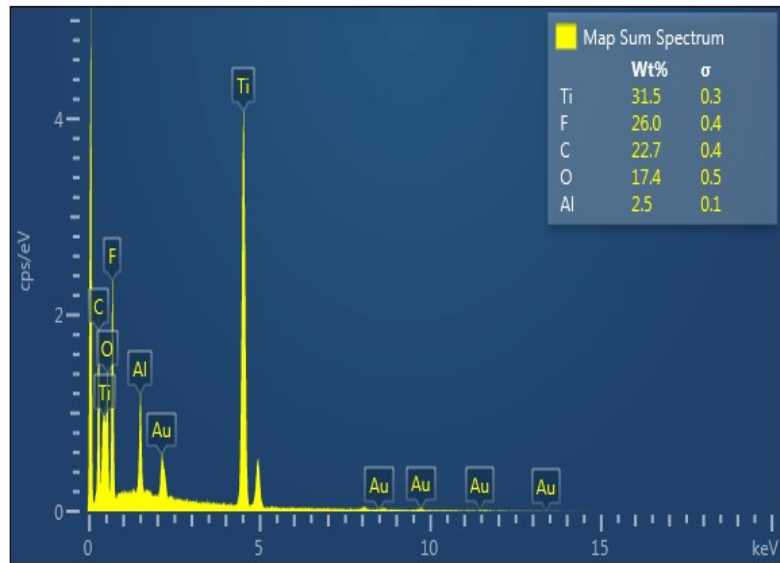


Figure S3. EDX spectra of $\text{Ti}_3\text{C}_2\text{T}_x$

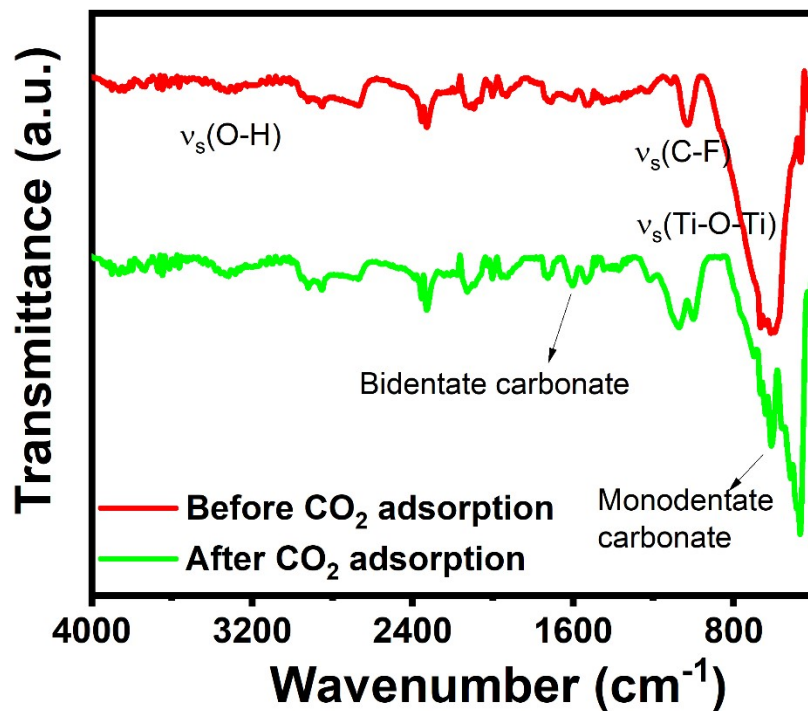


Figure S4. FT-IR spectra of $\text{Ti}_3\text{C}_2\text{T}_x$ before and after CO_2 adsorption

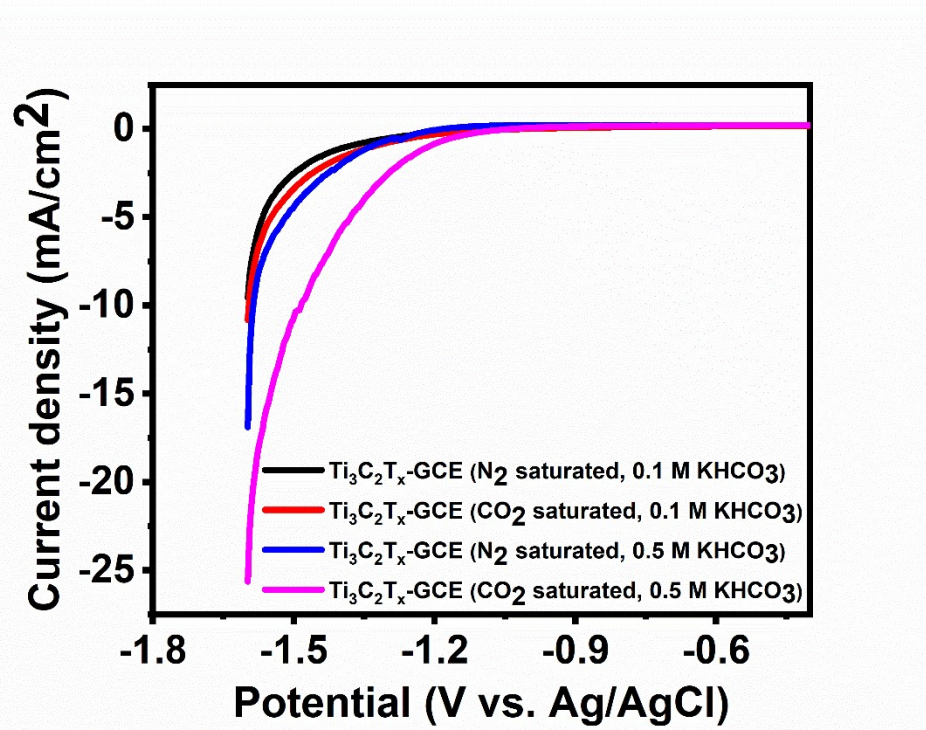


Figure S5. LSV curves comparison at two different electrolyte concentrations, 0.1 M KHCO_3 and 0.5 M KHCO_3 .

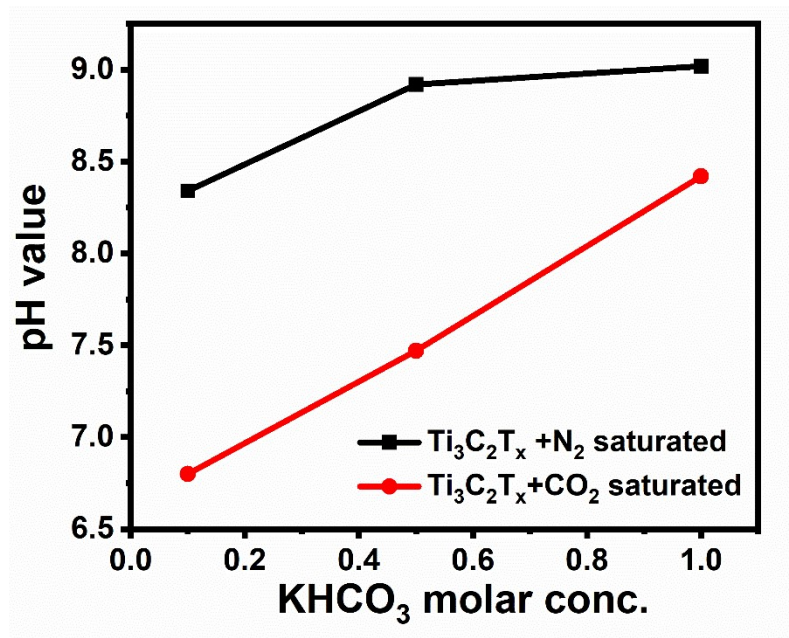


Figure S6. The pH values of the various concentration of KHCO_3 electrolytes before and after CO_2 purging

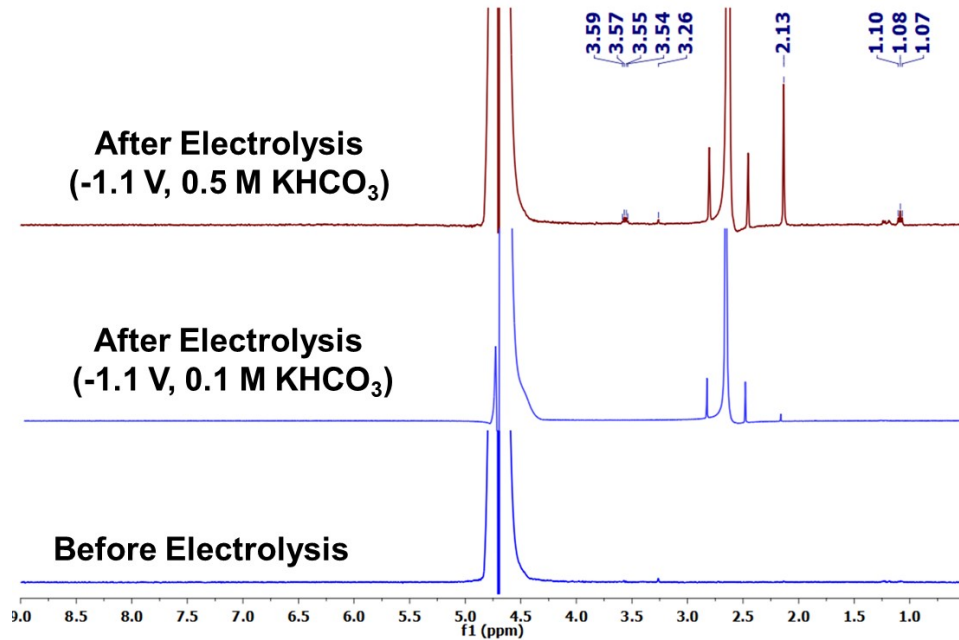


Figure S7. ¹H NMR spectra of electrolysis products formed in two different electrolyte concentrations before and after 3 h

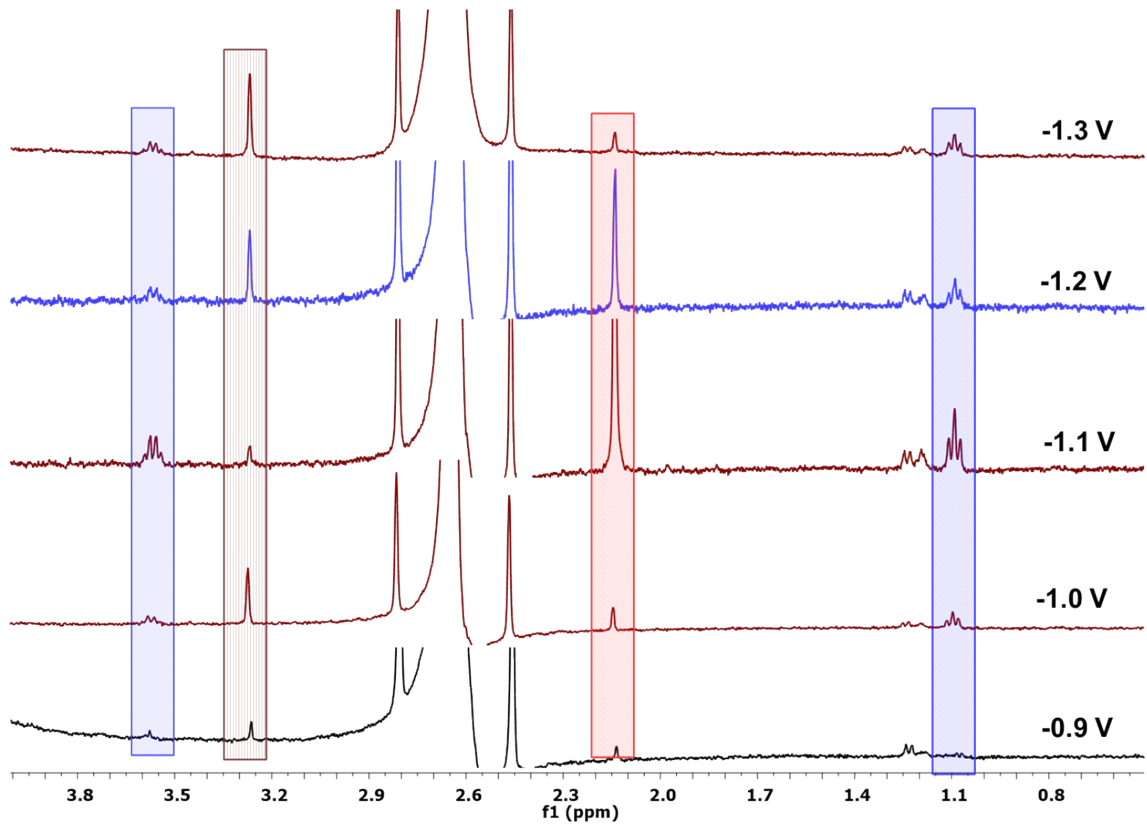


Figure S8. ^1H NMR spectra of products obtained from CA analysis with different potential (vs. Ag/AgCl) for 3 h.

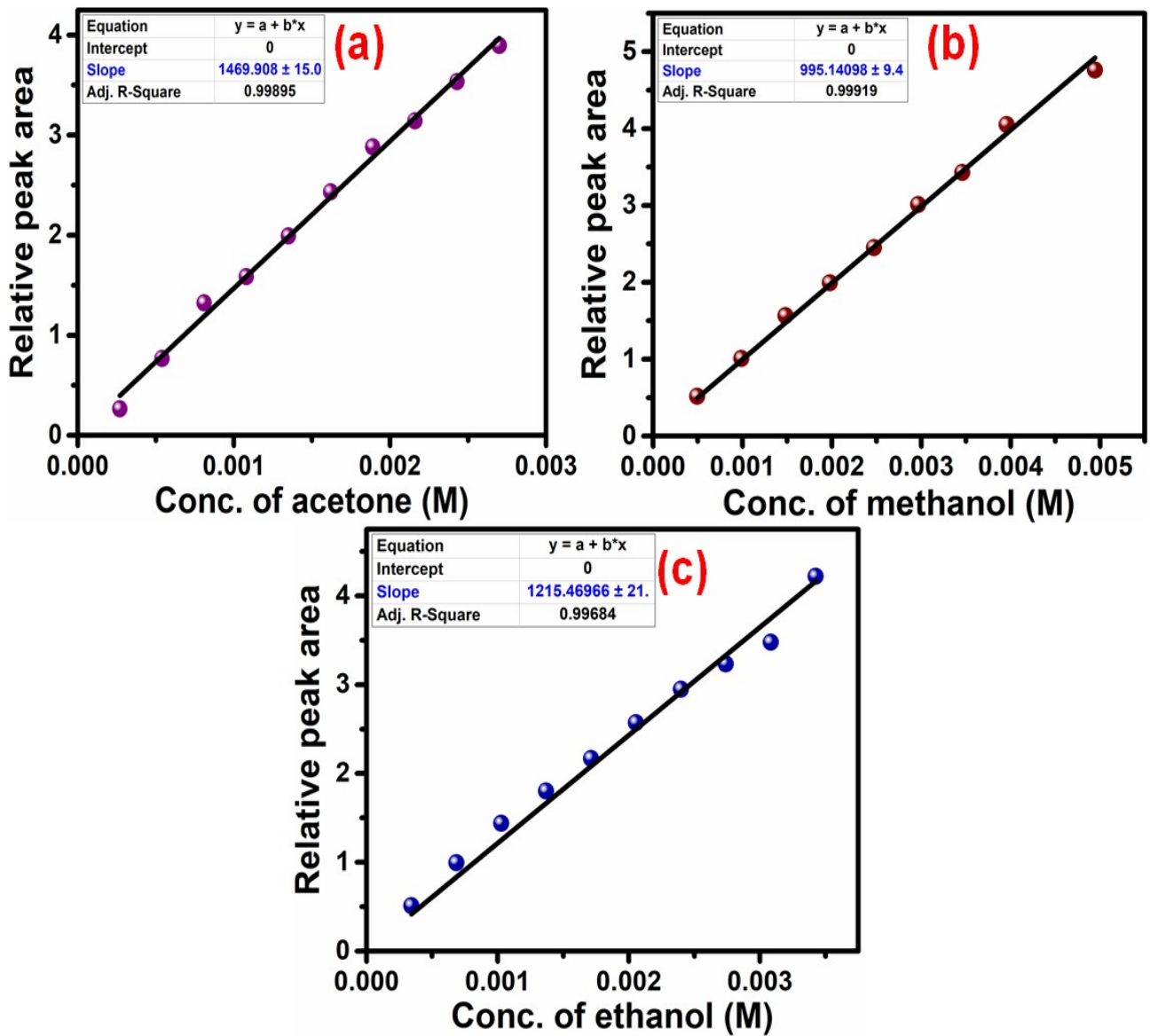


Figure S9. Linearly fitted standard calibration plots for (a) acetone, (b) methanol and (c) ethanol. The relative peak areas refer to ratios of $^1\text{H-NMR}$ peak areas (for methyl ($-\text{CH}_3$) protons) of the organic products (keeping a varying known concentration) with that of an internal standard DMSO (keeping a fixed known concentration) recorded in the identical solvent system as in the electrolysis.

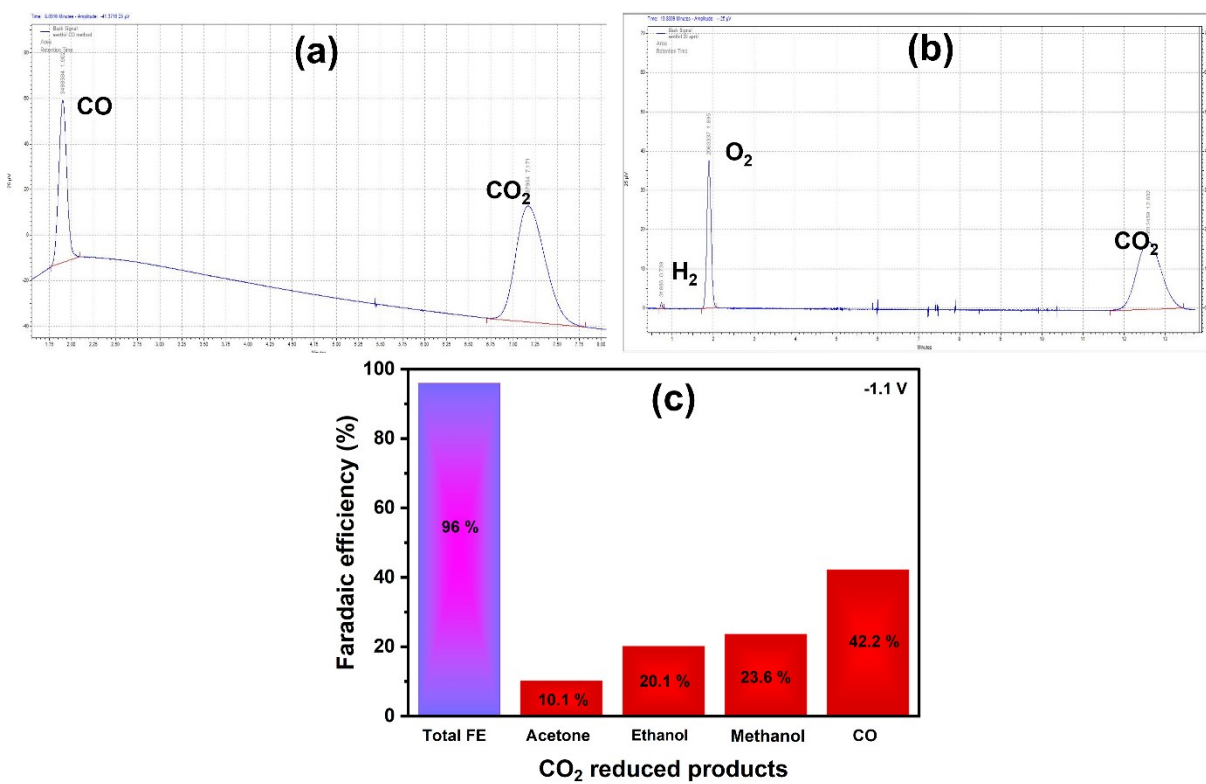


Figure S10. Gas chromatography profiles showing the formation of (a) CO, (b) H₂ and (c) overall CO₂-reduced products carried out at the constant potential of -1.1 V (vs. Ag/AgCl) for 3 h.

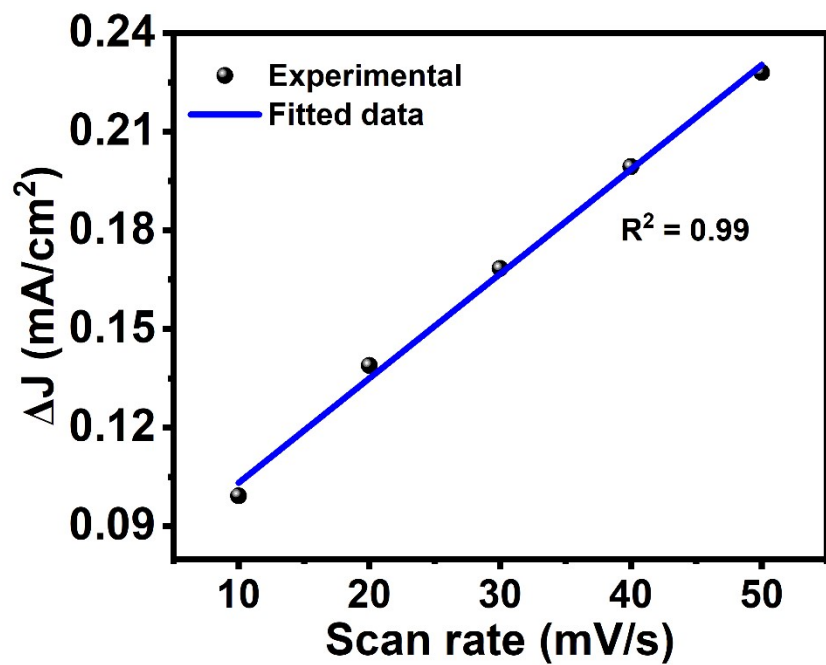


Figure S11. Electrochemical double layer plot (Scan rate vs. ΔJ) of modified $\text{Ti}_3\text{C}_2\text{T}_x$ -GCE

Table S1. Electrocatalytic properties $\text{Ti}_3\text{C}_2\text{T}_x$ -GCE with recently reported 2D materials

towards C_1 and C_{2+} products.

Electrocatalysts	Electrolyte	Operating potential	Products	Faradaic efficiency	References
t					es
$\text{Ti}_3\text{C}_2\text{T}_x$ -GCE	0.5 M KHCO_3	-0.45 V (vs RHE)	Ethanol, Methanol & Acetone	96 %	This work
Ti_2CT_x	Acetonitrile+ DI water+ BMIMBF_4	-1.8 V (vs SHE)	HCOOH	56.1 %	¹
N-doped Ti_3C_2	Seawater	-0.7 V (vs RHE)	CO	92 %	²
$\text{Mo}_2\text{C} \& \text{Ti}_3\text{C}_2$	(1-ethyl-2-methylimidazolium tetrafluoroborate)	-2.5 V (vs SHE)	CO	90 % & 65 %	³
$\text{Cu}/\text{Ti}_3\text{C}_2\text{T}_x$	1M KOH	-0.7 V (vs RHE)	C_2H_4 , EtOH & acetate	71 %, 25 % & 2.2 %	⁴
$\text{Ti}_3(\text{Al}_{1-x}\text{Cu}_x)\text{Cu}$	0.1M KHCO_3	-1.4 V (vs SHE)	CH_3OH	59.1 %	⁵
BiOBr templated catalyst	0.1M KHCO_3	-1.0 V (vs RHE)	Formate	90 %	⁶

Sn sheets confined graphene	0.1M NaHCO ₃	-1.8 V (vs SHE)	Formate	89 %	7
2D SnO ₂	0.1M NaHCO ₃	-1.13 V (vs RHE)	Formate	90 %	8
SnO ₂ @ N- doped nanocarbon	0.1M KHCO ₃	-1.2 V (vs RHE)	Formate	93.2 %	9
Bi ₂ O ₃	0.5M KHCO ₃	-0.9 V (vs RHE)	Formate	91 %	10
Cu nanosheets	2 M KOH	-	Acetate	48 %	11
SnO ₂ on CuO	0.5M KHCO ₃	-1.0 V (vs RHE)	C ₂ H ₄	22 %	12
Cu-Cu ₂ O	0.1M KHCO ₃	-1.1 V (vs RHE)	C ₂ H ₄	36 %	13
Pd/SnO ₂	0.1M NaHCO ₃	-0.26 V (vs RHE)	CH ₃ OH	34 %	14
CuO/TiO ₂	0.1M KHCO ₃	-0.85 V (vs RHE)	EtOH, acetone &acetate	47.4 %	15

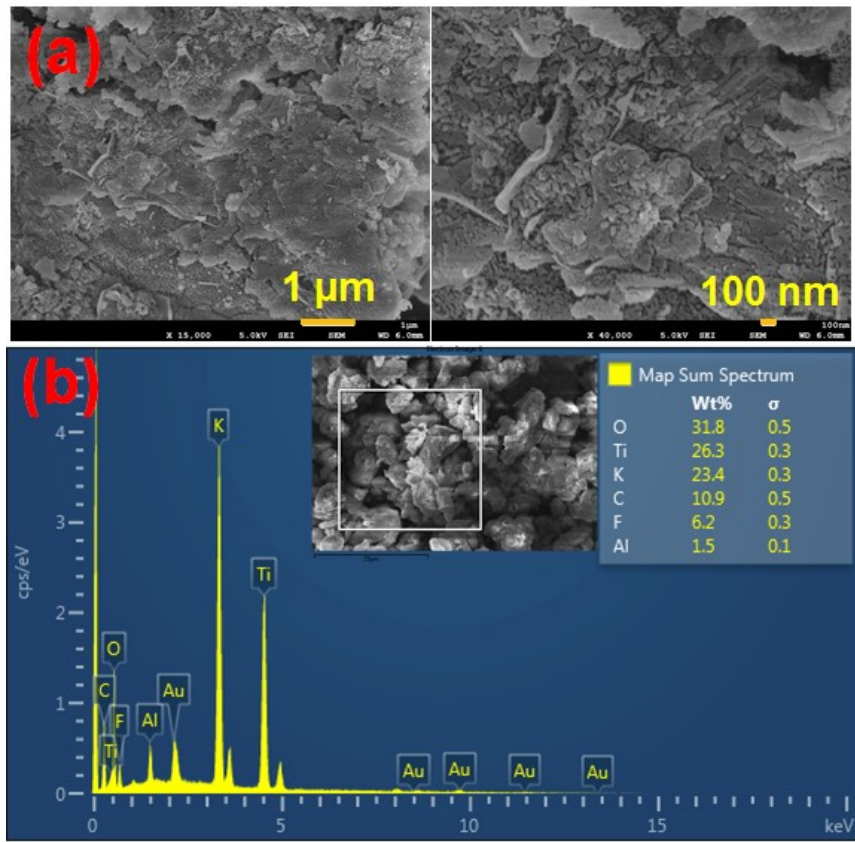


Figure S12. (a) FE-SEM and (b) EDX spectrum of $\text{Ti}_3\text{C}_2\text{T}_x$ -GCE after 72 h of electrocatalysis

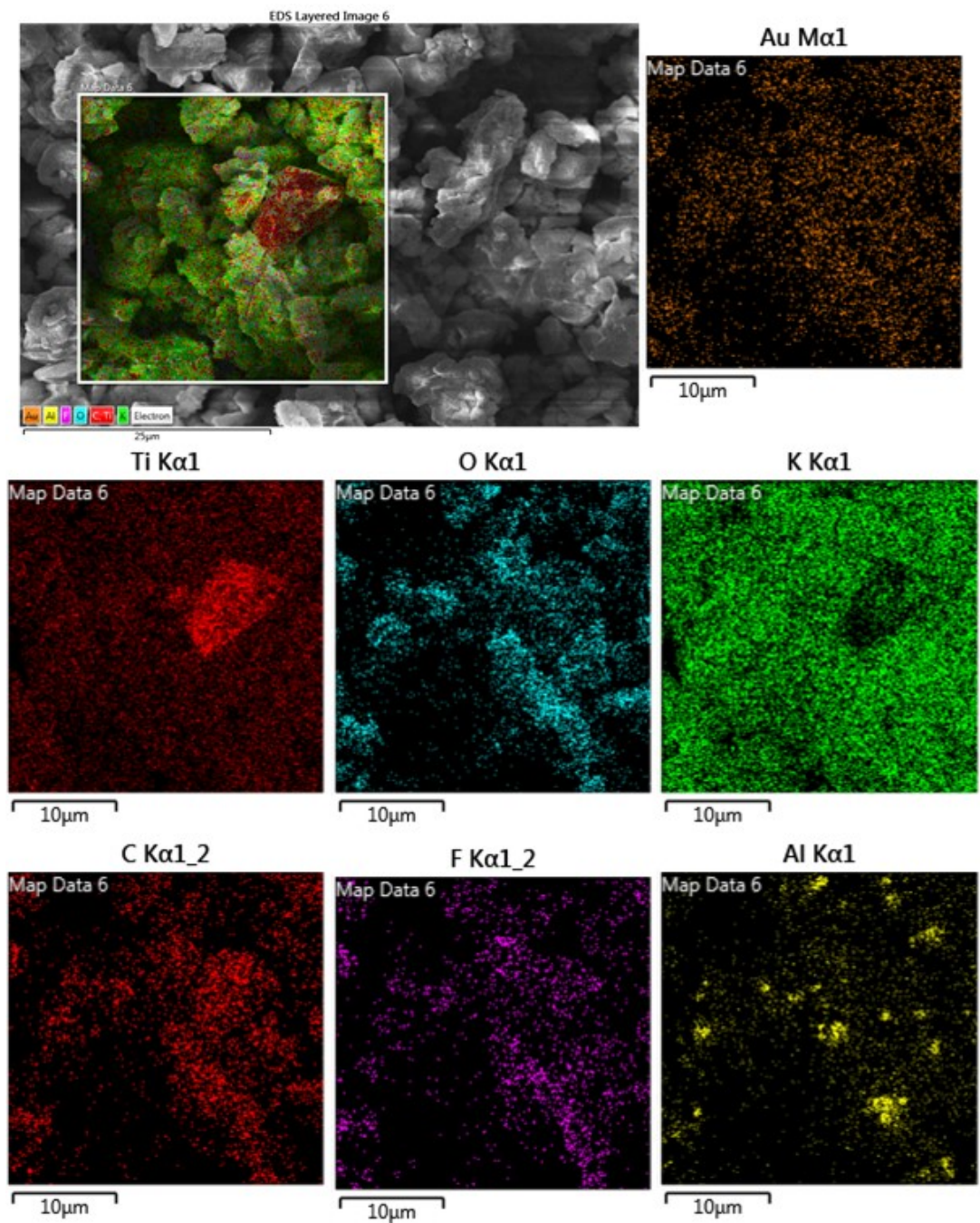


Figure S13. Elemental mapping of $\text{Ti}_3\text{C}_2\text{T}_x$ -GCE after 72 hr stability studies

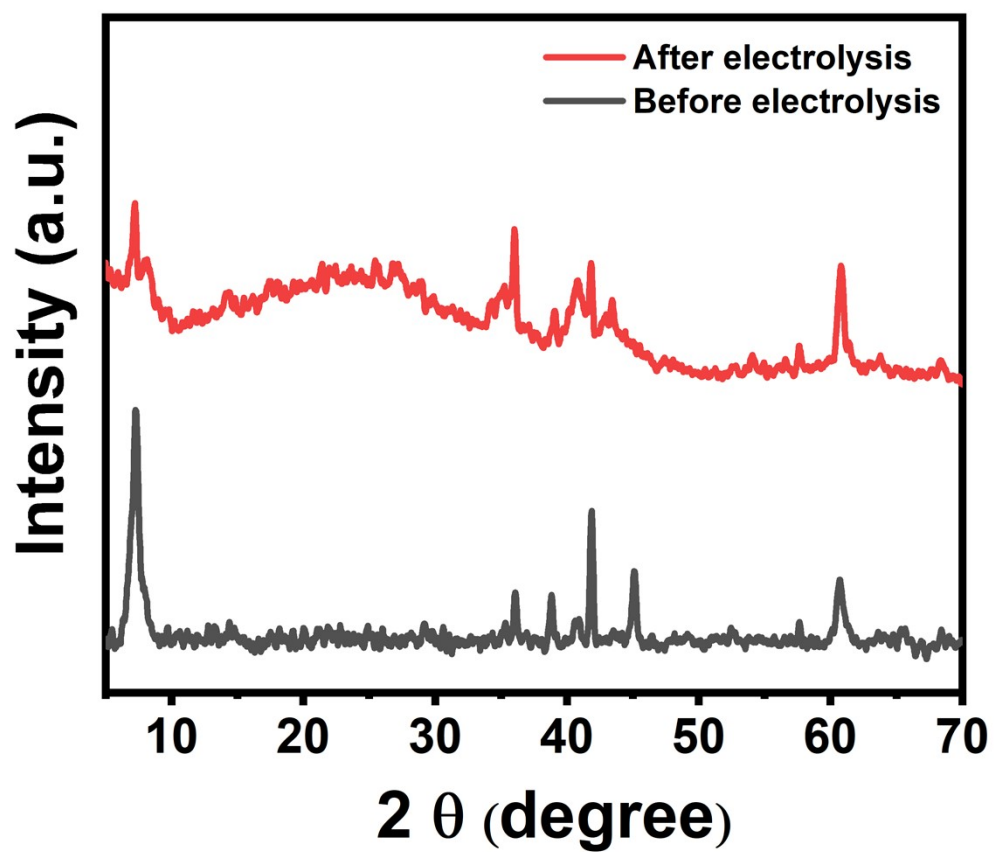


Figure S14. P-XRD pattern of $\text{Ti}_3\text{C}_2\text{T}_x$ before and after 72 hr electrolysis

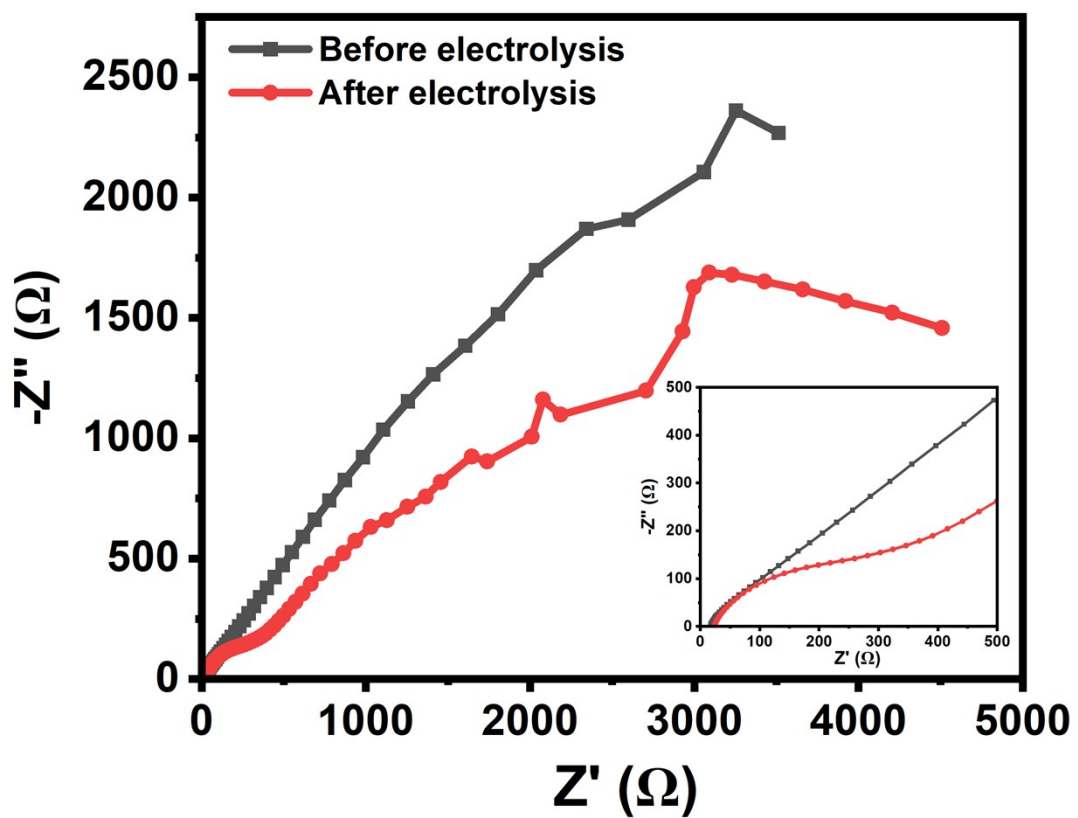


Figure S15. Electrochemical impedance spectroscopy (EIS) of $\text{Ti}_3\text{C}_2\text{T}_x$ -GCE before and after 72 hr electrolysis

References

- 1 A. D. Handoko, H. Chen, Y. Lum, Q. Zhang, B. Anasori and Z. W. Seh, *iScience*, 2020, **23**, 101181.
- 2 D. Qu, X. Peng, Y. Mi, H. Bao, S. Zhao, X. Liu and J. Luo, *Nanoscale*, 2020, **12**, 17191–17195.
- 3 N. H. Attanayake, H. R. Banjade, A. C. Thenuwara, B. Anasori, Q. Yan and D. R. Strongin, *Chemical Communications*, 2021, **57**, 1675–1678.
- 4 H. Bao, Y. Qiu, X. Peng, J. ao Wang, Y. Mi, S. Zhao, X. Liu, Y. Liu, R. Cao, L. Zhuo, J. Ren, J. Sun, J. Luo and X. Sun, *Nat Commun*, 2021, **12**, 1–9.
- 5 Q. Zhao, C. Zhang, R. Hu, Z. Du, J. Gu, Y. Cui, X. Chen, W. Xu, Z. Cheng, S. Li, B. Li, Y. Liu, W. Chen, C. Liu, J. Shang, L. Song and S. Yang, *ACS Nano*, 2021, **15**, 4927–4936.
- 6 F. P. García de Arquer, O. S. Bushuyev, P. De Luna, C. T. Dinh, A. Seifitokaldani, M. I. Saidaminov, C. S. Tan, L. N. Quan, A. Proppe, M. G. Kibria, S. O. Kelley, D. Sinton and E. H. Sargent, *Advanced Materials*, 2018, **30**, 6–11.
- 7 F. Lei, W. Liu, Y. Sun, J. Xu, K. Liu, L. Liang, T. Yao, B. Pan, S. Wei and Y. Xie, *Nat Commun*, 2016, **7**, 1–8.
- 8 J. Li, J. Jiao, H. Zhang, P. Zhu, H. Ma, C. Chen, H. Xiao and Q. Lu, *ACS Sustain Chem Eng*, 2020, **8**, 4975–4982.
- 9 Y. Fu, T. Wang, W. Zheng, C. Lei, B. Yang, J. Chen, Z. Li, L. Lei, C. Yuan and Y. Hou, *ACS Appl Mater Interfaces*, 2020, **12**, 16178–16185.
- 10 P. Deng, H. Wang, R. Qi, J. Zhu, S. Chen, F. Yang, L. Zhou, K. Qi, H. Liu and B. Y. Xia, *ACS Catal*, 2020, **10**, 743–750.
- 11 W. Luc, X. Fu, J. Shi, J. J. Lv, M. Jouny, B. H. Ko, Y. Xu, Q. Tu, X. Hu, J. Wu, Q. Yue, Y. Liu, F. Jiao and Y. Kang, *Nat Catal*, 2019, **2**, 423–430.
- 12 Y. Lan, G. Niu, F. Wang, D. Cui and Z. Hu, *ACS Appl Mater Interfaces*, 2020, **12**, 36128–36136.
- 13 N. Altaf, S. Liang, L. Huang and Q. Wang, *Journal of Energy Chemistry*, 2020, **48**, 169–180.
- 14 W. Zhang, Q. Qin, L. Dai, R. Qin, X. Zhao, X. Chen, D. Ou, J. Chen, T. T. Chuong, B. Wu and N. Zheng, *Angewandte Chemie - International Edition*, 2018, **57**, 9475–9479.
- 15 J. Yuan, J. J. Zhang, M. P. Yang, W. J. Meng, H. Wang and J. X. Lu, *Catalysts*, , DOI:10.3390/catal8040171.